BIOCHEMISTRY
including biophysical chemistry & molecular biology
Article

Biochemistry **2009,** *48,* 5239–5245 5239
DOI: 10.1021/bi900456e

Structure−Function Analyses of Isochorismate-Pyruvate Lyase from *Pseudomonas aeruginosa* Suggest Differing Catalytic Mechanisms for the Two Pericyclic Reactions of This Bifunctional Enzyme[†]

Qianyi Luo, Jose Olucha, and Audrey L. Lamb*

Department of Molecular Biosciences, University of Kansas, Lawrence, Kansas 66045

Received March 16, 2009; Revised Manuscript Received May 11, 2009

ABSTRACT: The isochorismate-pyruvate lyase from *Pseudomonas aeruginosa* (PchB) catalyzes two pericyclic reactions in a single active site. PchB physiologically produces salicylate and pyruvate from isochorismate for ultimate incorporation of the salicylate into the siderophore pyochelin. PchB also produces prephenate from chorismate, most likely due to structural homology to the *Escherchia coli* chorismate mutase. The molecular basis of catalysis among enzymatic pericyclic reactions is a matter of debate, one view holding that catalysis may be derived from electrostatic transition state stabilization and the opposing view that catalysis is derived from the generation of a reactive substrate conformation. Mutant forms of PchB were generated by site-directed mutagenesis at the site (K42) hypothesized to be key for electrostatic transition state stabilization (K42A, K42Q, K42E, and K42H). The loop containing K42 is mobile, and a mutant to slow loop dynamics was also designed (A43P). Finally, a previously characterized mutation (I87T) was also produced. Circular dichroism was used to assess the overall effect on secondary structure as a result of the mutations, and X-ray crystallographic structures are reported for K42A with salicylate and pyruvate bound and for apo-I87T. The data illustrate that the active site architecture is maintained in K42A-PchB, which indicates that differences in activity are not caused by secondary structural changes or by differences in active site loop conformation but rather by the chemical nature of this key residue. In contrast, the I87T structure demonstrates considerable mobility, suggesting that loop dynamics and conformational plasticity may be important for efficient catalysis. Finally, the mutational effects on k_{cat} provide evidence that the two activities of PchB are not covariant and that a single hypothesis may not provide a sufficient explanation for catalysis.

The isochorismate-pyruvate lyase (IPL)[1] from *Pseudomonas aeruginosa* (PchB) physiologically catalyzes the elimination of the enolpyruvyl side chain from isochorismate to make salicylate for incorporation into the siderophore pyochelin (Figure 1a) (*1*). The IPL reaction is a concerted but asynchronous quantitative hydrogen transfer, with a pericyclic transition state (*2*). The structure of PchB was determined (*3*), confirming that this enzyme is a structural homologue of the *Escherichia coli* chorismate mutase (EcCM) (*4*). This structural similarity possibly accounts for residual chorismate mutase (CM) activity, albeit with considerably lower efficiency (*1*). This single-substrate chorismate mutase reaction has one chemical step: concerted bond breaking at the ether oxygen and formation of a bond between C1 and C9 with a cyclic transition state (Figure 1b) (*5*). Therefore, this one enzyme catalyzes two pericyclic reactions, unusual reactions in cellular metabolism, in a single active site.

Two structures have been reported for PchB (*3*), an apo structure in which the active site loop was disordered and a pyruvate-bound structure in which the active site loop was ordered and closed. Lys42 of the mobile active site loop hydrogen bonds to a pyruvate molecule that was hypothesized to bind to the site occupied by the pyruvate formed in the elimination reaction (*3*). Corresponding amino acids in EcCM (Lys39) and the *B. subtilis* chorismate mutase (BsCM) (Arg90) have been determined to be critical for catalysis by mutational analysis (*6*−*10*). Whereas it may be likely that PchB will perform the CM reaction using a mechanism similar to that seen for its structural homologue EcCM, it does not necessarily follow that PchB will use the same mechanism to perform the physiologically important IPL activity. Therefore, it is necessary to perform a complete steady state kinetic analysis of both the CM and IPL activities to identify a possible role for Lys42. Toward this end, we generated the following PchB mutant enzymes: K42A, K42E, K42Q, and K42H. We have also generated a mutation at a site adjacent to K42 in the active site loop. This mutation, A43P, inserts a rigid amino acid into the flexible active site loop to test the hypothesis that loop movement correlates to catalytic rates. In other words,

[†]This publication was made possible by funds from the American Lung Association of Kansas and from the Kansas Masonic Cancer Research Institute.

*To whom correspondence should be addressed. Phone: (785) 864-5075. Fax: (785) 864-5294. E-mail: lamb@ku.edu.

[1]Abbreviations: BsCM, *Bacillus subtilis* chorismate mutase; CM, chorismate mutase; EcCM, *Escherichia coli* chorismate mutase; IPL, isochorismate-pyruvate lyase; MjCM, *Methanococcus jannaschii* chorismate mutase; NAC, near attack conformation; PchB, isochorismate-pyruvate lyase from *Pseudomonas aeruginosa*.

Published on Web 05/11/2009

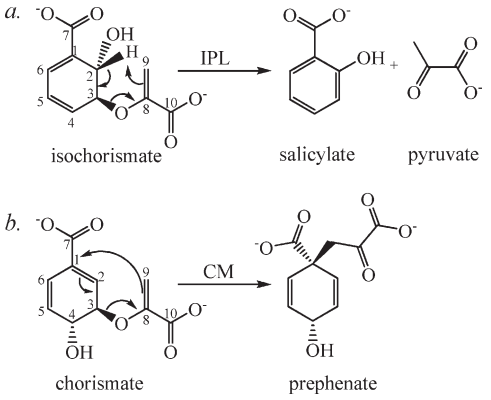

FIGURE 1: Catalytic activities of PchB: (a) isochorismate pyruvate lyase, a quantitative hydrogen transfer, and (b) chorismate mutase, a Claisen rearrangement.

Table 1: Primers for Site-Directed Mutagenesis

K42A	5′-GCG TCG CGC TTC GCG GCC AGC GAG GCG-3′
K42E	5′-GCG TCG CGC TTC GAG GCC AGC GAG GCG-3′
K42Q	5′-GCG TCG CGC TTC CAG GCC AGC GAG GCG-3′
K42H	5′-GCG TCG CGC TTC CAT GCC AGC GAG GCG-3′
A43P	5′-GCG TCG CGC TTC AAG CCG AGC GAG GCG GCG-3′
I87T	5′-C ATC CAC TGG TAC ACC GCC GAG CAG ATC-3′

we hypothesize that a mutant variety with a less flexible active site loop would exhibit slower catalytic rates. Finally, we generated the previously described I87T active site mutant (*1*), which was documented to have CM activity comparable to that of the wild type, but no detectable IPL activity.

The molecular basis for catalysis for enzymatic pericyclic reactions has been proposed by Bruice and his co-workers (*11*−*15*) to be derived from the formation of a reactive substrate conformation [termed the near attack conformation (NAC)]. The rotation of the pyruvylenol tail over the ring of the isochorismate (lyase reaction) or chorismate (mutase reaction) into an unfavorable, pseudodiaxial conformation is required to enhance the rate of reaction. This is accomplished by strategically placed arginines that align the two substrate carboxylates forming the reactive substrate conformation (*15*). Other computational results obtained by Mulholland and his co-workers (*16*−*19*) suggest that the formation of a reactive substrate conformation provides only a portion of the energy required to surpass the energy barrier, and that transition state stabilization is as important or even more important to catalysis. In each of the chorismate mutases, a charged amino acid (Arg or Lys) has been identified in the active site in the proximity of the ether oxygen of bond cleavage. This amino acid has been mutated to a variety of uncharged amino acids, resulting in a considerable decrease in catalytic efficiency (*6*−*10*, *20*). These results have supported the hypothesis that electrostatic transition state stabilization is required for catalysis. This idea has met with the criticism that changes in the active site at this amino acid may result in changes in active site architecture (*11*).

PchB provides an exciting platform for testing the competing hypotheses of electrostatic transition state stabilization versus reactive substrate conformation and a means of measuring the relative contributions of both mechanisms for catalytic enhancement of two pericyclic activities performed in the same active site. The first step toward this goal is to determine if mutational changes in the active site merely change the active site architecture or if instead the mutations provide a valid basis for determining the catalytic importance of particular amino acids. Herein, we describe the generation and characterization of the PchB active site mutants described above. We report the structural characterization of the mutant enzymes by circular dichroism and report the crystallographic structures of two of the active site mutants (K42A and I87T). We also compare the kinetic parameters of these mutants for both catalytic activities, including a discussion of the change in the free energy of activation of the mutants relative to that of the wild type.

EXPERIMENTAL PROCEDURES

Preparation of PchB and PchB Mutants. Wild-type PchB without a histidine tag was prepared as previously described (*3*). Site-directed mutants of PchB were prepared using the QuikChange kit (Stratagene, as per the manufacturer's instructions) with the plasmid generated for wild-type protein overexpression (*3*), and the primers listed in Table 1 (mutant codons underlined). All mutations were confirmed by sequence analysis (DNA Facility of the Iowa State University Office of Biotechnology, Ames, IA). The resultant plasmids encoding the *pchB* gene mutants were transformed individually into BL21(DE3) *E. coli* (Stratagene) for overproduction. Mutant protein overexpression and purification were performed as previously described for the wild-type PchB protein (*3*) with comparable yields of ~250 mg/L of *E. coli* culture.

Preparation of Isochorismate and Chorismate. Isochorismate was isolated from *Klebsiella pneumoniae* 62-1 harboring the *entC* plasmid pKS3-02 (*21*) with only minor changes. One significant change was the use of a Nucleosil 5 μm C18 100A column (250 mm × 21.2 mm; 5 μm). The concentration of isochorismate was determined by UV spectroscopy using an ε_{278} of 8300 M^{-1} cm^{-1}. Chorismate (Sigma, 60−80% pure) was recrystallized as previously described (*22*).

Circular Dichroism Spectroscopy. CD spectra of wild-type and mutant PchB enzymes [~2 μM protein in 20 mM sodium/potassium phosphate (pH 7.0)] were recorded with a Jasco (Easton, MD) J-815 spectrometer at 25 °C with a path length of 1 cm. Spectra were recorded five times for each sample and averaged. The step size and bandwidth were 1 nm, and the averaging time at each wavelength was 1 s.

Crystallization of K42A-PchB. Crystallization was carried out by the hanging drop method at 18 °C. Purified K42A-PchB (44 mg/mL) was incubated with 37 mM salicylate and 37 mM pyruvate on ice for 30 min. Drops containing 1 μL of this protein/reaction product solution were mixed with 2 μL of a well solution consisting of 0.1 M Tris-HCl (pH 8.5), 2 M ammonium phosphate, and 13% glycerol. Hexagonal pyramidal crystals grew to ~1 mm × 0.7 mm × 0.4 mm in one week.

Crystallization of I87T-PchB. I87T-PchB crystals were grown at 25 °C by the hanging drop method. Drops containing 1.5 μL of I87T-PchB (19 mg/mL) were mixed with 1.5 μL of reservoir solution composed of 0.1 M Bis-Tris propane (pH 6.5), 0.14 M calcium chloride, 23% PEG 3350, and 10% glycerol. Rectangular box crystals with dimensions of up to 0.4 mm × 0.06 mm × 0.05 mm were obtained in one week.

Collection of Crystallographic Data and Structure Determination for K42A-PchB. A K42A-PchB crystal was harvested from the drop and flash-cooled to −160 °C. Diffraction data were collected using a Rigaku RUH3R rotating anode generator equipped with an R-axis IV image plate detector at the University of Kansas Protein Structure Lab. The exposure time per image was 10 min with 1° oscillation steps and a crystal−detector distance of 150 mm. Diffraction data were indexed and scaled using the *hkl* program package (*23*). The structure was

Table 2: Crystallographic Statistics

	K42A with products	apo-I87T
Data Collection		
resolution range (Å)	41.5−2.5	100−2.15
space group	$P2_12_12_1$	$P2_12_12_1$
unit cell dimensions (Å)	a = 48.0, b = 53.2, c = 82.3	a = 54.5, b = 74.9, c = 88.5
no. of observations		
unique	7706	20232
total	50717	345137
completeness (%)[a]	99.9 (99.9)	99.2 (98.6)
R_{sym}[a,b]	0.101 (0.227)	0.108 (0.423)
% $>3\sigma(I)$[a]	85.7 (72.9)	80.4 (55.4)
Refinement		
resolution range (Å)	41.5−2.5	44.24−2.25
no. of reflections	7346	16778
R-factor[c]	0.218	0.219
R_{free}[d]	0.276	0.256
no. of dimers per asymmetric unit	1	2
no. of atoms		
protein, non-hydrogen	1580	2726
non-protein	48	77
root-mean-square deviation		
lengths (Å)	0.01	0.008
angles (deg)	1.22	1.02
overall B-factor (Å^2)	15.6	20.1
protein	15.8	20.1
ligands	12.3	−

[a] Values in parentheses are for the highest-resolution shell: 2.59−2.5 Å for K42A and 2.23−2.15 Å for I87T. [b] $R_{sym} = \sum|I_{obs} - I_{avg}|/\sum I_{obs}$, where the summation is over all reflections. [c] R-factor $= \sum||F_o| - |F_c||/\sum|F_o|$. [d] For calculation of R_{free}, 4.5% (K42A) and 5.1% (I87T) of the reflections were reserved.

determined with the molecular replacement program Phaser from the CCP4 program suite (*24*) using the PchB pyruvate-bound structure (Protein Data Bank entry 2H9D) as a model, with the water and ligands omitted. Model building and refinement were conducted with Coot (*25*) and REFMAC (*26*). The model includes residues 1 − 99 in each monomer, 16 water molecules, two salicylates, and two pyruvates. A Ramachandran plot generated in PROCHECK (*27*) shows that the model exhibits good geometry with 96.6% of the residues in the most favored regions, 2.8% in the additionally allowed regions, and 0.6% in the generously allowed regions. The amino acid that is generously allowed is Ala50 of the A chain, an active site loop amino acid in an area of poor electron density. Data collection and refinement statistics are listed in Table 2.

Collection of Crystallographic Data and Structure Determination for I87T-PchB. An I87T-PchB crystal was transferred to cryoprotectant solution containing 0.1 M Bis-Tris propane (pH 6.5), 0.2 M calcium chloride, 30% PEG 3350, and 20% glycerol and flash-cooled to −160 °C. Collection of data and structure determination were carried out as described for K42A-PchB. Included in the model are four monomers, each with varying flexibility in the active site loop (residues 39−51) and termini. Monomer A comprises residues 2−43 and 56−94. Monomer B comprises residues 10−41 and 51−93. Monomer C comprises residues 2−39 and 54−98. Monomer D comprises residues 2−98. The model also includes one calcium ion at a crystal contact and 76 water molecules. A Ramachandran plot generated in PROCHECK (*27*) shows that the model exhibits good geometry, with 99% of the residues in the most favored regions and 1% in the additionally allowed regions. Data collection and refinement statistics are listed in Table 2.

Structural Analysis. All root-mean-square deviations were calculated using LSQMAN in the DEJAVU program package (*28*). Protein structure figures were generated using PyMOL (*29*).

Protein Data Bank Submission. The atomic coordinates and structure factors (entries 3HGW and 3HGX) have been deposited in the Protein Data Bank, Research Collaboratory for Structural Bioinformatics, Rutgers University, New Brunswick, NJ.

Chorismate Mutase (CM) Activity Assays. Initial velocities of the CM reaction catalyzed by PchB and its mutants were determined by measuring the decrease in absorbance at 310 nm, which corresponds to the disappearance of chorismate (ε_{310} = 370 M^{-1} cm^{-1}), with a Cary 50 Bio spectrophotometer (Varian). The enzyme was incubated in 50 mM sodium/potassium phosphate buffer (pH 7.5) for 10 min at room temperature (22 °C). The reaction was initiated by the addition of chorismate, varied in concentration from 0.1 to 1.4 mM for the wild type and A43P and from 0.1 to 8 mM for K42A, K42H, and I87T. Kinetic data were fit to the Michaelis−Menten equation by the nonlinear regression function of SigmaPlot (SSPS, Inc.). The assay at pH 5.0 for K42H was performed as described above, except that the buffer was a multicomponent buffer containing 50 mM formate, 50 mM MES, and 100 mM TrisHCl adjusted to the desired pH with HCl (*30*).

Isochorismate Pyruvate Lyase (IPL) Assays. Initial velocities of the IPL reaction were determined by measuring the accumulation of salicylate by fluorescence with an excitation wavelength of 300 nm and an emission wavelength of 430 nm using a Cary Eclipse fluorescence spectrophotometer (Varian). The reactions were assessed in 50 mM sodium/potassium phosphate (pH 7.5) at room temperature and initiated by the addition of isochorismate, varied in concentration from 1 to 80 μM for the wild type, I87T, and A43P and from 5 to 390 μM for K42A, K42H, and K42Q. The amount of salicylate formed was determined from a standard curve with a varied salicylate concentration (0−80 μM) in the reaction buffer. Kinetic data were fit to the Michaelis−Menten equation by the nonlinear regression function of KaleidaGraph (Synergy Software). The assay at pH 5.0 for K42H was performed as described above, except that the buffer was a multicomponent buffer described for the chorismate mutase assay.

Preparation of $\Delta\Delta G^{\ddagger}$ Plots. The "mutational effect" recorded in Table 3 was determined by dividing the k_{cat} or k_{cat}/K_m of the mutant enzyme by that of the wild type. The points on the $\Delta\Delta G^{\ddagger}$ plots were calculated from the equation

$$\Delta\Delta G^{\ddagger} = -RT \ln(\text{mutational effect})$$

RESULTS

Secondary Structure Maintained As Detected by Circular Dichroism Spectroscopy. Circular dichroism spectroscopy was used to assess the secondary structure of the mutant proteins. All six mutated proteins were found to be comparable to the wild type with strong minima at 208 and 212 nm, characteristic of helical structure (Figure 2).

Active Site Architecture of K42A-PchB Maintained. The structure of the K42A mutant with salicylate and pyruvate bound

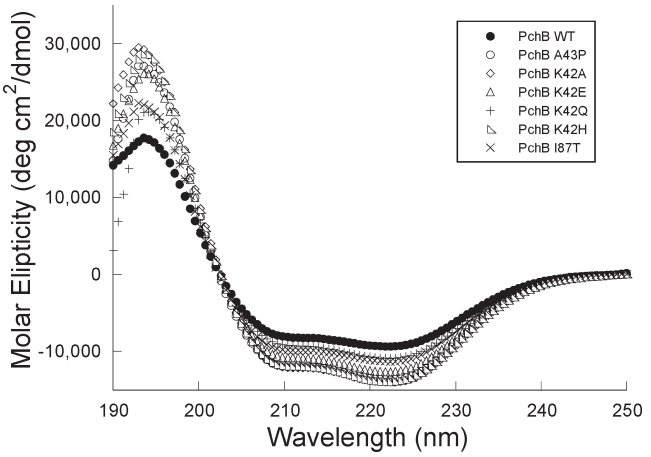

FIGURE 2: Circular dichroism spectra of PchB and mutants, demonstrating maintained helical structure. It should be noted that the PchB mutants at K42 did not produce a shoulder at ~210 nm as documented for comparable mutants in EcCM (*9*), a feature that has been used to argue that the EcCM mutant proteins are not structurally intact.

in the active site was determined to 2.5 Å. Whereas the K42A and pyruvate-bound wild-type (*3*) proteins crystallized in the same space group ($P2_12_12_1$), the unit cells were significantly different. The K42A structure has only one dimer per asymmetric unit, as opposed to two in the wild-type crystal, and has a significantly smaller unit cell (>150000 Å^3 smaller). In the K42A structure, both active sites are closed, and each contained one salicylate and one pyruvate. We previously hypothesized by wrong-ligand crystallographic modeling (*3*) that the salicylate binds more deeply than pyruvate in the active site pocket. In this experiment (*3*), each of the pyruvates was individually substituted with salicylate and both models were subjected to simulated annealing. Only in the case in which the salicylate carboxylate was aligned by Arg31 was a reasonable hydrogen bonding pattern maintained with this modeling procedure. In the K42A mutant structure, the carboxylate of the salicylate is indeed aligned in the active site by the side chain of Arg31, and the pyruvate is aligned in the active site by Arg14 as predicted. The wild-type and K42A active sites are overlaid in Figure 3A. The root-mean-square deviation (rmsd) for the monomer displayed is 0.43 Å for 98 α-carbons (of the 99 in the K42A structure) and for the dimer is 0.58 Å for 197 α-carbons, which demonstrates the expected overall conservation of structure between the wild type and the mutated enzyme. The architecture of the active site is conserved in the mutated enzyme despite the differences in crystal systems and previously documented flexibility in this loop. The rmsd for the α-carbon at the 42 position is 0.21 Å in the monomer displayed and 0.46 Å in the opposing monomer, which had somewhat less well-defined density. A stereoimage of the active site is displayed in Figure 3C to further emphasize that the active sites of the K42A mutant enzyme and the wild type overlay with surprising exactness, and that changes in activity are not the result of subtle changes in active site architecture.

Increased Flexibility of the I87T-PchB Active Site. In contrast to K42A, the apo-I87T protein crystallized in the same crystal system (space group and unit cell) of the previously published pyruvate-bound wild-type (WT) structure (*3*) and also contained two dimers per asymmetric unit. Despite this similarity, only one of the four active sites was closed (Figure 4A). The remaining active sites had disordered active site loops (Figure 4B), as previously documented for the apo-wild-type structure. However, the apo-I87T structure is more mobile than that seen in previous PchB structures, and the disorder is not confined to the active site loop (amino acids 39−51) in some of the monomers. Previously documented structures with open active sites have disorder from amino acid 42 to amino acids 47−51, depending on the monomer. The I87T structure has three open active sites of the four in the two dimers, and disorder begins at residues 40−44 and continues until residues 50−55. This means not only that the loop is disordered in most monomers but also that there is some unwinding of the helix following the loop, specifically in monomers A and C.

Flexibility of the Active Site Is Not Linked to Crystallization Buffers, Precipitants, or the Unit Cell. Four structures of PchB have now been reported, two here and two previously (*3*). While it might be tempting to hypothesize that increased loop flexibility in these structures is correlated to pH or precipitant, this is not the case. First, all four crystallized from different mother liquors ranging in pH from 4.7 (apo-WT structure) to 8.5 (K42A structure). The most disordered structure is of intermediate pH (6.5, I87T). Second, the precipitants for crystallization were PEG3350 (I87T and pyruvate-bound WT) and salts (nitrate for apo-WT and phosphate for K42A), with both precipitant groups containing ordered and disordered active site loops. The two structures that crystallized from PEG3350 (I87T and wild type with pyruvate bound) have isomorphous crystal systems, yet in no case is the active site loop involved in a crystal packing interface, which could thereby potentially cause closing or deformation of this loop. Therefore, we conclude that active site loop flexibility is not a function of crystallization.

Changes in k_{cat}/K_m Due to Active Site Mutation Show a Surprising Level of Correlation. The k_{cat}/K_m for both the IPL and CM activities measured for the wild-type enzyme is ~4-fold lower than that reported previously (*1*). This result is most likely caused by several differences in how the enzyme was produced and purified, and in the how the assays were conducted. The most probable reason for the difference is the temperature at which the assays were conducted: our assays were conducted at 22 °C instead of 37 °C. Since the goal of this work is to compare wild-type to mutated enzymes and for this work all enzyme preparations and assays were done comparably, the differences between this work and that done previously do not change the conclusions drawn.

All of the Lys42 mutations caused a significant reduction in activity for both IPL and CM activity (Table 3). The K42E mutation changes the side chain charge from positive to negative, and the mutated form of the enzyme showed no detectable activity in either assay; whereas the K42Q mutation had detectable activity only in the IPL assay. For the variants at the K42 site with detectable activity, the changes in activity were all comparable with a decrease of ~100-fold in k_{cat}/K_m. In other words, the mutational effects ranged from 0.01 to 0.04. The mutational effect for the A43P (in the flexible loop) and I87T (active site) mutations were less pronounced. For all of the mutations that had both IPL and CM activity, the $\Delta\Delta G^{\ddagger}$ values of the mutational effect are plotted in Figure 5A. This plot shows a surprising level of correlation such that the active site changes yield changes in k_{cat}/K_m that are covariant for the two activities. The linear regression produces a line with a slope of 0.93 ± 0.15 and an R^2 value of 0.92.

Changes in k_{cat} Due to Active Site Mutation Are Not Correlated. The mutations resulted in more varied effects

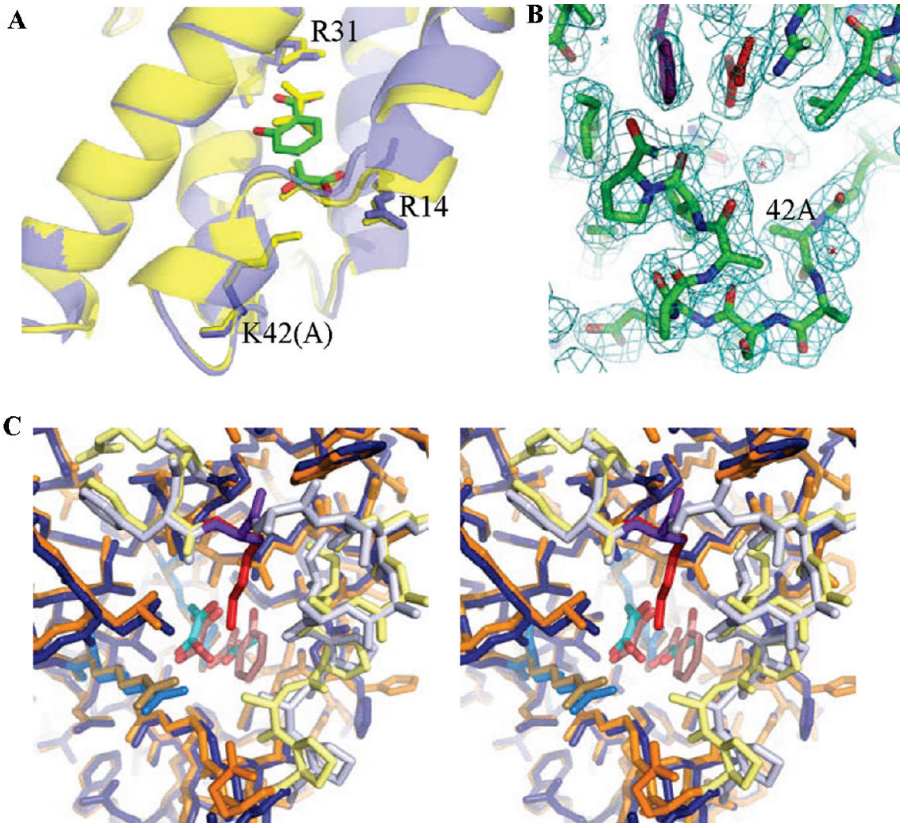

FIGURE 3: K42A structure. (A) Cartoon of the K42A active site (light purple) superimposed on WT (yellow) (Protein Data Bank entry 2H9D) highlighting conservation of secondary structure and active site loop conformation. The salicylate and pyruvate molecules of the K42A structure are shown as green sticks with red oxygens, and the pyruvates of the wild-type structure are shown as yellow sticks. (B) An electron density map of the K42A active site highlights the loop that is mobile in the open structures of PchB. The salicylate is colored purple, and the pyruvate is colored red. (C) Stereodiagram of the superimposed WT and K42A active sites displaying the conservation of active site architecture. For WT, the sticks are colored orange with the active site loop colored yellow; for K42A, the sticks are colored dark blue with the active site loop colored light purple (thereby somewhat conserving the color system of panel A). K42 is colored red and K42A dark purple. The brown (WT) and aquamarine (K42A) sticks are arginines 14 and 31 that align the substrates. The pyruvates of the WT structure are colored cyan with red oxygens, and the salicylate and pyruvate of the K42A structure are colored pink with red oxygens.

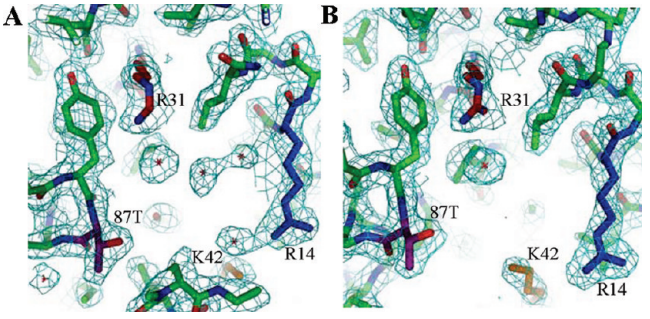

FIGURE 4: Comparison of I87T molecules. (A) Electron density map of the monomer D active site of I87T with the active site loop ordered (bottom). (B) Electron density map of the monomer A active site of I87T with the active site loop (residues 44−55) disordered. In both panels, Arg31 is colored red, Arg14 blue, Lys42 orange, and Thr87 (of the I87T mutation) purple. In the two active sites, Lys42 is in different positions, with the position in panel A (monomer D) equivalent to that observed in the pyruvate-bound wild-type structure.

for k_{cat}. For example, the K42 mutations all caused consistent decreases in IPL activity, but the CM activity for the same mutations ranged from complete abrogation of activity to a k_{cat} similar to 2-fold higher than that of the wild type. The two other active site mutations were comparable to WT (A43P; both activities) to a mutational effect of 2.89 for I87T CM activity, but 0.08 for IPL activity. These data are more easily visualized in the $\Delta\Delta G^{\ddagger}$ of the mutational effect plot of Figure 5B. Clearly, the mutational effect on k_{cat} is not covariant for the two activities. The linear regression produces a line with a slope of 0.15 ± 0.41 and an R^2 value of 0.04.

DISCUSSION

Active Site Maintained in K42 Mutants. Lys39 of EcCM (comparable to Lys42 in PchB) has been identified as an amino acid important in stabilizing the developing negative charge at the ether oxygen of the pyruvylenol tail during bond breaking in a polar transition state (*9*). However, the CD spectra of mutated EcCM with changes at this site had a small shoulder at ~210 nm (*9*), leading to arguments that decreased activity in chorismate mutases altered at this site is due to changes in the active site architecture (*11*, *12*). Clearly, this does not hold for PchB: the CD spectra of the K42 mutants are predominantly α-helical and have spectra comparable to that of the wild type (Figure 2). Furthermore, the structures of K42A-PchB and the wild type have active sites equivalent in shape, and the salicylate and pyruvate are in comparable binding modes (Figure 3C). Therefore, the ~100-fold decrease in k_{cat}/K_m for the CM and IPL activities of the K42A-PchB mutated enzyme must be a result of the change in the side chain at this position.

I87T-PchB Is More Flexible than Wild-Type PchB. Unlike the previous report (*1*), we do find PchB-I87T to be IPL active, instead having an only ~3-fold decrease in k_{cat}/K_m relative to that of the wild type. Whereas this mutant does retain

Table 3: Steady State Kinetic Parameters for PchB and Active Site Mutants

	chorismate mutase activity					isochorismate-pyruvate lyase activity				
	K_m (μM)	k_{cat} ($\times 10^{-3}$ s^{-1})	mutational effect[a]	k_{cat}/K_m (M^{-1} s^{-1})	mutational effect[a]	K_m (μM)	k_{cat} ($\times 10^{-3}$ s^{-1})	mutational effect[a]	k_{cat}/K_m (M^{-1} s^{-1})	mutational effect[a]
wild type	120 ± 10	23.5 ± 0.5		196		4.3 ± 0.2	177 ± 2		41100	
K42A	720 ± 30	1.5 ± 0.00	0.06	2	0.01	51 ± 3	24.5 ± 0.5	0.14	480	0.01
K42E	[b]	[b]				[b]	[b]			
K42Q	[b]	[b]				66 ± 3	46.8 ± 0.8	0.26	709	
K42H (pH 7.5)	3770 ± 40	26.8 ± 0.3	1.14	7	0.04	57 ± 2	37.0 ± 0.7	0.21	650	0.02
K42H (pH 5.0)	5800 ± 100	48 ± 3	2.04	8	0.04	66 ± 1	118 ± 7	0.67	17900	0.04
A43P	186 ± 2	26.2 ± 0.2	1.11	141	0.72	5.3 ± 0.1	188 ± 5	1.06	35500	0.86
I87T	440 ± 20	68 ± 1	2.89	155	0.79	1.09 ± 0.05	14.2 ± 0.3	0.08	13000	0.32

[a] (Mutant value)/(wild-type value). [b] Below the limits of detection (8 μM for the CM assay and 0.03 μM for the IPL assay).

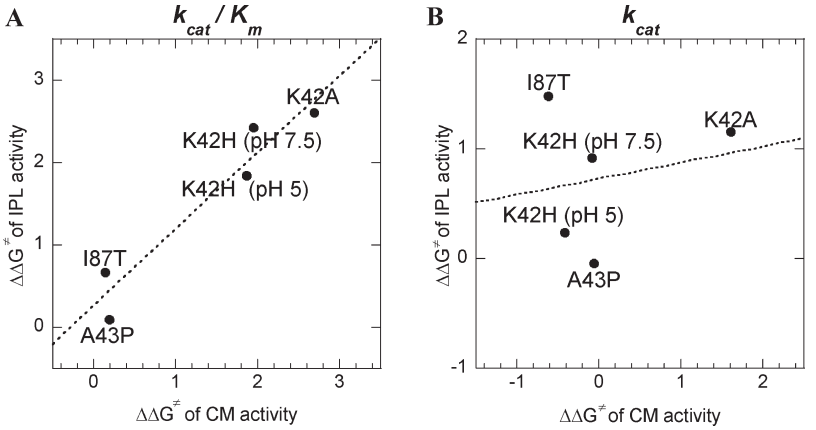

FIGURE 5: Mutational effect on k_{cat}/K_m (A) and k_{cat} (B). The points on the $\Delta\Delta G^{\ddagger}$ plots were calculated as described in the experimental procedures for each mutant protein that displayed both chorismate mutase and isochorismate-pyruvate lyase activities. (A) The linear regression produces a line with the equation $y = 0.93x + 0.26$ (slope of ±0.15, intercept of ±0.26) and an R^2 value of 0.92, demonstrating a clear correlation between the mutational effects on the two activities. (B) In contrast, there is no correlation between the mutational effects on k_{cat}, since the linear regression produces a line with the equation $y = 0.15x + 0.74$ (slope of ±0.41, intercept of ±0.32) and an R^2 value of 0.04.

nearly wild-type CM activity, the enzyme is still nearly 100-fold more efficient as a lyase than as a mutase. Gaille et al. (*1*) hypothesized that the change in activities is due to the differing alignment of the substrates in the active site due to H-bonding with the threonine. Since chorismate lacks a hydroxyl at the 2-position (Figure 1) necessary for H-bonding to the threonine, there should be no change in the binding mode of this substrate because of the mutation. This could be an explanation for the difference in activities that we observe, with nonproductive binding of isochorismate (the 2-OH hydrogen bonding to the threonine at the 87 position) causing the more significant change in the IPL k_{cat}/K_m. The structure does not have ligands bound, so we cannot promote or discount this hypothesis; however, we can offer a second hypothesis. I87T-PchB is the most mobile of the PchB structures determined, and the mobility is not limited to the active site loop. The N-terminus of the α-helix following the active site loop is also disordered. This change in protein flexibility may also contribute to the changes in activity. Flexibility in a chorismate mutase with a fold comparable to that of PchB has been documented previously (*31*−*34*). Hilvert and co-workers generated a monomeric form of the *Methanococcus jannaschii* chorismate mutase (MjCM) through mutations in the C-terminal helix and in the N-terminal long helix such that the long helix folds over to complete the active site. This functional monomer is catalytic with an only 3-fold decrease in activity relative to that of wild-type MjCM and is predominantly a molten globule unless a substrate or a transition state analogue is present.

Mutational Effects on k_{cat}/K_m for the CM and IPL Activities Are Covariant, whereas Those for k_{cat} Are Not. The PchB variants exhibited a surprising level of correlation in mutational effects between the lyase and mutase activities when k_{cat}/K_m were compared (Figure 5A), with the exception of the K42Q mutation which was IPL active and CM deficient. The high correlation with unit slope suggests that each mutation produces a unique change in transition state free energy that is shared by both IPL and CM transition states. Consequently, in the rate-determining step for k_{cat}/K_m, both transition states (CM and IPL) are structurally and electrostatically similar. This is appropriate for the electrostatic transition state hypothesis, but if a near attack conformation is involved in k_{cat}/K_m, then the NAC must form between the reactant state and the transition state. In contrast, the two activities are decidedly not covariant with respect to k_{cat} (Figure 5B). The lack of correlation is derived from a structural lack of similarity between reactant states and/or transition states, suggesting most simply that neither a reactive substrate conformation nor electrostatic transition state stabilization completely accounts for the rate-determining step for k_{cat}, but perhaps there are differing mixtures of the two.

CONCLUSIONS

PchB is a unique enzyme that performs two pericyclic reactions: a physiological lyase activity and an adventitious mutase activity. A debate in the field concerning chorismate mutases

suggests that the arginines deep in the active site cavity are necessary and sufficient for catalysis, organizing the substrates for catalysis (reactive substrate conformation or near attack conformation). In the opposing view, substrate organization is viewed as an effect of the formation of the enzyme−substrate complex and the lysine at the 42 position is required for activity (electrostatic transition state stabilization). We show by CD and X-ray crystallographic methods that the changes in activity after mutation at the 42 site are not due to the change in active site architecture but are an effect of the side chain at the 42 position. Whereas mutation of the comparable amino acids to Lys42 in BsCM and EcCM led to complete abrogation of catalytic activity, we show that for similar mutations in PchB activity decreases by only 100-fold. The A43P-PchB mutant designed to increase the rigidity of the active site loop had small mutational effects, suggesting that loop dynamics at the active site may play a role in catalysis. A formerly characterized mutation (I87T) caused considerable protein disorder which may account for the mutational effects. While the lysine at position 42 certainly aids in enzymatic efficiency, activity was detectable in mutants without a positive charge at this site. The mutational effects on CM and IPL k_{cat}/K_m are covariant; however, mutational effects on k_{cat} are not. Catalysis by PchB cannot be solely explained by either of the two extreme hypotheses for enzymatic pericyclic reactions. Instead, the IPL and CM activities are most likely the result of a mixture of the formation of a reactive substrate conformation and electrostatic transition state stabilization.

ACKNOWLEDGMENT

We are grateful to Drs. T. C. Gamblin and R. N. De Guzman for equipment use and to Dr. R. L. Schowen for insightful discussions. Special thanks to Drs. M. Buechner, R. H. Himes, and E. E. Scott for critically reading the manuscript.

REFERENCES

1. Gaille, C., Kast, P., and Haas, D. (2002) Salicylate biosynthesis in *Pseudomonas aeruginosa*. Purification and characterization of PchB, a novel bifunctional enzyme displaying isochorismate pyruvate-lyase and chorismate mutase activities. *J. Biol. Chem. 277*, 21768–21775.
2. DeClue, M. S., Baldridge, K. K., Kunzler, D. E., Kast, P., and Hilvert, D. (2005) Isochorismate Pyruvate Lyase: A Pericyclic Reaction Mechanism?. *J. Am. Chem. Soc. 127*, 15002–15003.
3. Zaitseva, J., Lu, J., Olechoski, K. L., and Lamb, A. L. (2006) Two crystal structures of the isochorismate pyruvate lyase from *Pseudomonas aeruginosa*. *J. Biol. Chem. 281*, 33441–33449.
4. Lee, A. Y., Karplus, P. A., Ganem, B., and Clardy, J. (1995) Atomic structure of the buried catalytic pocket of *Escherichia coli* chorismate mutase. *J. Am. Chem. Soc. 117*, 3627–3628.
5. Gustin, D. J., Mattei, P., Kast, P., Wiest, O., Lee, L., Cleland, W. W., and Hilvert, D. (1999) Heavy Atom Isotope Effects Reveal a Highly Polarized Transition State for Chorismate Mutase. *J. Am. Chem. Soc. 121*, 1756–1757.
6. Cload, S. T., Liu, D. R., Pastor, R. M., and Schultz, P. G. (1996) Mutagenesis Study of Active Site Residues in Chorismate Mutase from *Bacillus subtilis*. *J. Am. Chem. Soc. 118*, 1787–1788.
7. Kast, P., Asif-Ullah, M., Jiang, N., and Hilvert, D. (1996) Exploring the active site of chorismate mutase by combinatorial mutagenesis and selection: The importance of electrostatic catalysis. *Proc. Natl. Acad. Sci. U.S.A. 93*, 5043–5048.
8. Kast, P., Grisostomi, C., Chen, I. A., Li, S., Krengel, U., Xue, Y., and Hilvert, D. (2000) A strategically positioned cation is crucial for efficient catalysis by chorismate mutase. *J. Biol. Chem. 275*, 36832–36838.
9. Liu, D. R., Cload, S. T., Pastor, R. M., and Schultz, P. G. (1996) Analysis of Active Site Residues in *Escherichia coli* Chorismate Mutase by Site-Directed Mutagenesis. *J. Am. Chem. Soc. 118*, 1789–1790.
10. Zhang, S., Kongsaeree, P., Clardy, J., Wilson, D. B., and Ganem, B. (1996) Site-directed mutagenesis of monofunctional chorismate mutase engineered from the *E. coli* P-protein. *Bioorg. Med. Chem. 4*, 1015–1020.
11. Hur, S., and Bruice, T. C. (2002) The mechanism of catalysis of the chorismate to prephenate reaction by the *Escherichia coli* mutase enzyme. *Proc. Natl. Acad. Sci. U.S.A. 99*, 1176–1181.
12. Hur, S., and Bruice, T. C. (2003) The near attack conformation approach to the study of the chorismate to prephenate reaction. *Proc. Natl. Acad. Sci. U.S.A. 100*, 12015–12020.
13. Hur, S., and Bruice, T. C. (2003) Just a near attack conformer for catalysis (chorismate to prephenate rearrangements in water, antibody, enzymes, and their mutants). *J. Am. Chem. Soc. 125*, 10540–10542.
14. Hur, S., and Bruice, T. C. (2003) Comparison of formation of reactive conformers (NACs) for the Claisen rearrangement of chorismate to prephenate in water and in the *E. coli* mutase: The efficiency of the enzyme catalysis. *J. Am. Chem. Soc. 125*, 5964–5972.
15. Zhang, X., Zhang, X., and Bruice, T. C. (2005) A definitive mechanism for chorismate mutase. *Biochemistry 44*, 10443–10448.
16. Claeyssens, F., Harvey, J. N., Manby, F. R., Mata, R. A., Mulholland, A. J., Ranaghan, K. E., Schutz, M., Thiel, S., Thiel, W., and Werner, H. J. (2006) High-accuracy computation of reaction barriers in enzymes. *Angew. Chem., Int. Ed. 45*, 6856–6859.
17. Claeyssens, F., Ranaghan, K. E., Manby, F. R., Harvey, J. N., and Mulholland, A. J. (2005) Multiple high-level QM/MM reaction paths demonstrate transition-state stabilization in chorismate mutase: Correlation of barrier height with transition-state stabilization. *Chem. Commun.,* 5068–5070.
18. Ranaghan, K. E., and Mulholland, A. J. (2004) Conformational effects in enzyme catalysis: QM/MM free energy calculation of the 'NAC' contribution in chorismate mutase. *Chem. Commun.,* 1238–1239.
19. Ranaghan, K. E., Ridder, L., Szefczyk, B., Sokalski, W. A., Hermann, J. C., and Mulholland, A. J. (2004) Transition state stabilization and substrate strain in enzyme catalysis: Ab initio QM/MM modelling of the chorismate mutase reaction. *Org. Biomol. Chem. 2*, 968–980.
20. Kienhofer, A., Kast, P., and Hilvert, D. (2003) Selective stabilization of the chorismate mutase transition state by a positively charged hydrogen bond donor. *J. Am. Chem. Soc. 125*, 3206–3207.
21. Schmidt, K., and Leistner, E. (1995) Microbial Production of (+)-*trans*-Isochorismic Acid. *Biotechnol. Bioeng. 45*, 285–291.
22. Rieger, C. E., and Turnbull, J. L. (1996) Small scale biosynthesis and purification of gram quantities of chorismic acid. *Prep. Biochem. Biotechnol. 26*, 67–76.
23. Otwinowski, Z., and Minor, W. (1997) Processing of X-ray Diffraction Data Collected in Oscillation Mode. *Methods Enzymol. 276*, 307–326.
24. McCoy, A. J., Grosse-Kunstleve, R. W., Storoni, L. C., and Read, R. J. (2005) Likelihood-enhanced fast translation functions. *Acta Crystallogr. D61*, 458–464.
25. Emsley, P., and Cowtan, K. (2004) Coot: Model-building tools for molecular graphics. *Acta Crystallogr. 60*, 2126–2132.
26. Winn, M. D., Isupov, M. N., and Murshudov, G. N. (2001) Use of TLS parameters to model anisotropic displacements in macromolecular refinement. *Acta Crystallogr. 57*, 122–133.
27. Laskowski, R., MacArthur, M., Moss, D., and Thornton, J. (1993) PROCHECK: A program to check the stereochemical quality of protein structures. *J. Appl. Crystallogr. 26*, 283–291.
28. Kleywegt, G. J., and Jones, T. A. (1997) Detecting folding motifs and similarities in protein structures. *Methods Enzymol. 277*, 525–545.
29. DeLano, W. (2002) The PyMOL Molecular Graphics System , DeLano Scientific, San Carlos, CA.
30. Gondry, M., Lautru, S., Fusai, G., Meunier, G., Menez, A., and Genet, R. (2001) Cyclic dipeptide oxidase from *Streptomyces noursei*. Isolation, purification and partial characterization of a novel, amino acyl α,β-dehydrogenase. *Eur. J. Biochem. 268*, 1712–1721.
31. MacBeath, G., Kast, P., and Hilvert, D. (1998) Redesigning enzyme topology by directed evolution. *Science 279*, 1958–1961.
32. Pervushin, K., Vamvaca, K., Vogeli, B., and Hilvert, D. (2007) Structure and dynamics of a molten globular enzyme. *Nat. Struct. Mol. Biol. 14*, 1202–1206.
33. Vamvaca, K., Jelesarov, I., and Hilvert, D. (2008) Kinetics and thermodynamics of ligand binding to a molten globular enzyme and its native counterpart. *J. Mol. Biol. 382*, 971–977.
34. Woycechowsky, K. J., Choutko, A., Vamvaca, K., and Hilvert, D. (2008) Relative tolerance of an enzymatic molten globule and its thermostable counterpart to point mutation. *Biochemistry 47*, 13489–13496.